

Minimal cyclic behavior in sheared amorphous solids

Chloe W. Lindeman* and Sidney R. Nagel

*Department of Physics and The James Franck and Enrico Fermi Institutes
The University of Chicago, Chicago, IL 60637, USA.*

(Dated: March 5, 2024)

Although jammed packings of soft spheres exist in potential-energy landscapes with a vast number of minima, when subjected to cyclic shear they may revisit the same configurations repeatedly. Simple hysteretic spin models, in which particle rearrangements are represented by spin flips, capture many features of this periodic behavior. Yet it has been unclear to what extent individual rearrangements can be described by such binary objects. Using a particularly sensitive algorithm, we identify rearrangements in simulated jammed packings. We select pairs of rearrangements that undo one another to create periodic cyclic behavior, explore the statistics of these pairs, and show that their internal structure is more complex than a spin analogy would indicate. This offers insight into both the collective nature of rearrangement events themselves and how complex systems such as amorphous solids can reach a limit cycle with relative ease.

Introduction — Athermal jammed packings of N repulsively interacting soft spheres exist in complex potential-energy landscapes in which each particle can move in d dimensions. In this Nd -dimensional parameter space there are a vast number of local energy minima corresponding to stable particle configurations. Shearing such a packing causes discontinuous rearrangements between stable configurations.

Surprisingly, when the shear is *cyclic*, these systems may reach a periodic orbit in which precisely the same configurations are revisited in each cycle; this is a physical memory of the driving [1]. Moreover, this periodic path in the energy landscape is often encountered after only a few cycles of applied shear. This has been seen in experiments and in simulations with and without friction in systems as large as 40,000 particles and with many rearrangements per cycle [2–9]. The fundamental question remains of how such periodicity emerges, and why it emerges after relatively few cycles of driving.

Previous work considered the possibility that each rearrangement, or plastic event, is a transition in a bistable system that can be undone upon reversal of the shear direction [10]. The transition on increasing strain occurs at a larger value than when the strain is decreased. This implies a region of strain, γ_h , over which there are two distinct stable states. In this region, the system is hysteretic and the configuration depends on the history of deformation (see Fig. 1a).

Indeed, hysteretic bistable elements first studied in the context of magnetic materials and Ising models [12, 13], called *hysteron*s, have become widely used to model particle rearrangements in cyclically driven disordered materials [14–19]. While ensembles of independent hysteron s exhibit similar kinds of memory as amorphous solids [14, 15, 18], details of the reversibility of individual rearrangements in jammed systems remain untested.

To add to the complexity, though independent hysteron s can lead to exceedingly complex trajectories through phase space [16, 17, 19–21], they cannot produce the long transients or multi-cycle periodicity observed in jammed systems without the presence of interactions between hysteron s [9, 18, 22, 23]. The notion of hysteron interactions necessitates that one be able to distinguish between a rearrangement — the “core” of a single hysteron — and the interactions — the “dressing” — between two rearranging entities. If this is not possible, then the non-interacting hysteron may not be an appropriate starting point to model memory formation in jammed packings.

Analysis of rearrangement pairs is thus necessary not only to bolster the connection between the complex energy landscape of jammed systems and the simple model of hysteretic spins, but also to understand the nature of inter-hysteron interactions. Here we investigate rearrangements in small packings of spheres, $7 \leq N \leq 257$. We focus on small system sizes with the aim of resolving each rearrangement and find correlations between energy, root-mean-square displacement, and (in the case of paired rearrangements) hysteresis.

To isolate the minimal elements for periodic response, we restrict our study to configurations in which the first instability encountered after a packing is created is undone by the first one found upon reversing the shear direction. Such rearrangement pairs are common: about half of all initial rearrangements are undone as described above. We also find that the distribution of strain intervals over which two stable configurations exist, $P(\gamma_h)$, is peaked at small values. Paired and unpaired rearrangements appear to be fundamentally similar to one another, suggesting that our measurements are indicative of the generic strain response, not specific to hysteron formation. To find the core of each hysteron, we measure the number of particles needed to push the system from one configuration to the other. This offers insight into the behavior of pairs at strains *between* the two rearrangements, complementing the statistics of the

* cwindeman@uchicago.edu

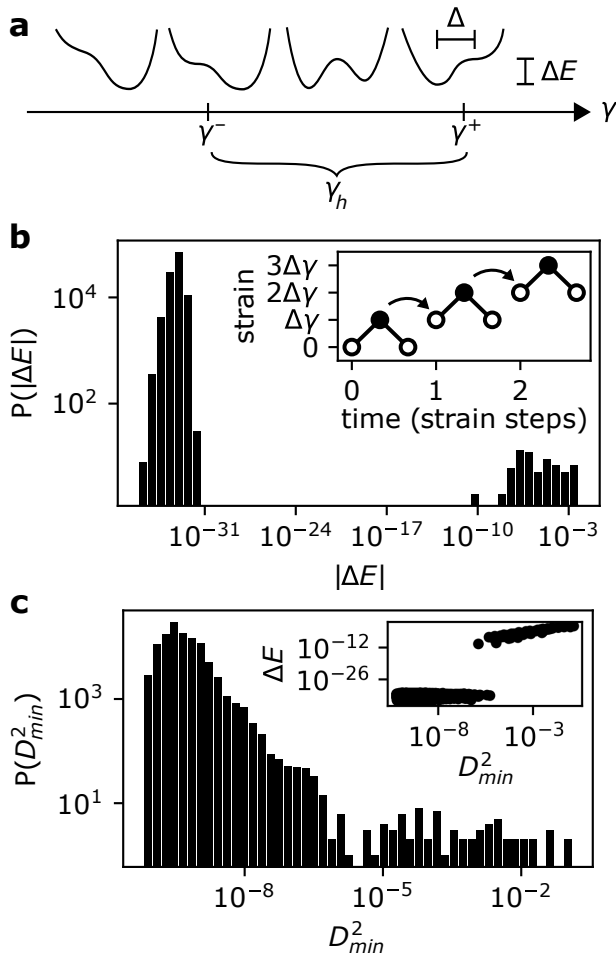


FIG. 1. (a) Illustration of hysteresis produced by a double-energy well modified by applied strain. At two critical values of strain, γ^- and γ^+ , the left and right wells flatten out, respectively; two stable minima exist for strains between these values. The distance $\gamma_h \equiv \gamma^+ - \gamma^-$ is a measure of hysteresis. Changes in particle position Δ and energy ΔE at an instability are depicted schematically. (b) Distribution, $P(|\Delta E|)$, of changes in absolute value of the energy upon returning to the same strain after one strain step. Reversible events have $|\Delta E| < 10^{-31}$ and are well separated from true rearrangements which have $|\Delta E| > 10^{-12}$. System had $N = 31$, $\phi = 0.87$ and $\Delta\gamma = 10^{-5}$. Inset shows method to find $|\Delta E|$ by comparing energies of adjacent open circles. (c) For same set of events, distribution of the corresponding D_{min}^2 values for sequential frames. Inset: ΔE versus D_{min}^2 . Clearly, $P(|\Delta E|)$ is much better at discriminating rearrangements from background than D_{min}^2 or the energy change between adjacent frames (shown in [11]).

rearrangements themselves.

Methods — We study two-dimensional packings of soft repulsive disks with periodic boundaries under athermal quasistatic shear using the pyCudaPacking package [24, 25]. The energy is defined by:

$$V(r_{ij}) = \epsilon(1 - r_{ij}/\sigma_{ij})^\alpha \Theta(\sigma_{ij} - r_{ij})$$

where ϵ is the energy scale, ij label particles separated by distance r_{ij} , $\sigma_{ij} \equiv \sigma_i + \sigma_j$ is the sum of particle radii, and $\Theta(x)$ is the Heaviside function. The exponent $\alpha = 2.5$ (Hertzian contacts) is chosen in order to avoid anomalous instabilities [26]. Packings are created at fixed packing fraction $0.87 \leq \phi \leq 0.99$ and radii are chosen from a log-normal distribution with 20% polydispersity. An initial configuration is generated with random particle positions (infinite temperature) and minimized using the Fast Inertial Relaxation Engine (FIRE). To apply shear, we set the lattice vectors of our periodic boundaries as specified in the SI and move each particle affinely before minimizing with FIRE.

In order to identify a rearrangement, we choose a strain step, $\Delta\gamma$, and at every step test for reversibility: we shear forward one strain step then shear backward by the same amount and calculate the magnitude of the energy change, $|\Delta E|$, at the same strain before and after that step, as indicated schematically in the inset to Fig. 1b (energy is compared between the connected pairs of open circles). As shown in Fig. 1b, rearrangements are well-defined; the magnitude of $|\Delta E|$ is either quad-precision error, $< 10^{-31}$, or $> 10^{-12}$. For the same set of events, such a separation is not found for other metrics such as the non-affine deformation D_{min}^2 [10], shown in Fig. 1c, or the energy change between adjacent frames (see [11]). In both those cases, a continuous range of the x -axis variable makes it impossible to identify with certainty when a rearrangement has occurred. After recording $|\Delta E|$, the system is reset to the configuration at the higher value of strain (indicated in the inset by an arrow) and the process is repeated.

For each packing, we increase the strain until we find a rearrangement. We then decrease the strain until another rearrangement is found and test whether these two rearrangements form a closed orbit. If so, the packing is considered a “hysteron” and is saved along with information about both rearrangements. If not, the packing is discarded and a new configuration is generated. Additionally, if at any point the strain exceeds a threshold $\gamma = 0.3$, or if at any point the entire packing loses rigidity, the packing is discarded. Additionally, if the particle radii are such that a particle interacts with the same neighbor on both sides (an issue only in the smallest packings $N = 7$), we choose new radii from the log-normal distribution. Our method of finding a rearrangement relies on irreversibility; in particular, a rearrangement pair with γ_h smaller than the step size $\Delta\gamma$ would be identified as reversible on the scale of the step size and hence entirely missed in our search protocol. We therefore repeat our search for hystérons using different values of the strain step size: $10^{-5} \leq \Delta\gamma \leq 10^{-3}$.

Statistics of rearrangement pairs — Using the relative number of packings saved versus those discarded, we calculate the probability $P(N)$ that a randomly generated packing with N particles will result in a rearrangement pair. Figure 2a shows that $P(N)$ has a slow (nearly logarithmic) decrease in the probability of finding paired re-

arrangements. Recall that we consider only pairs found immediately, with no other rearrangements in between. Thus these numbers are a lower bound on the fraction of rearrangements that can be undone.

We compute the probability that the two rearrangements are separated by a given strain γ_h , a measure of hysteresis, shown as a probability distribution function in Fig. 2b for 31-particle systems. The probability is sharply peaked at small hysteresis values – in all of the systems studied, the most probable γ_h was the smallest possible value, set by the step size $\Delta\gamma$. In such cases, the probability distribution $P(\gamma_h)$ is approximately exponential: $P(\gamma_h) \propto e^{-\gamma_h/\lambda}$, providing a characteristic strain scale λ over which the probability decays. Figure 2c shows that λ decreases with system size N : $\lambda \propto N^{-1}$. The hysteresis γ_h of a rearrangement pair found in a small system is typically larger than that found in a larger system.

Even after decreasing the step size by two orders of magnitude and increasing the typical pressure by a factor of ~ 20 , which tends to increase the distance to an instability, the most probable γ_h was still the smallest measurable. The inset to Fig. 2b shows this behavior for the smallest step size and largest packing fraction measured, $\Delta\gamma = 10^{-5}$ and $\phi = 0.99$.

The hysteresis values γ_h range over three decades, calling into question whether hysteron pairs with small and large γ_h are fundamentally different from each other. In order to answer this, we compute the root-mean-square displacement of all the particles during each rearrangement:

$$\Delta \equiv \left(\sum_i (\Delta r_i)^2 \right)^{1/2},$$

where Δr_i is the distance the i^{th} particle moved during the instability. Figures 3a and 3b show that the root-mean-squared displacement Δ and energy change ΔE vary smoothly with the hysteresis γ_h . Both Δ and ΔE show a strong correlation with the hysteresis: paired rearrangements with little hysteresis tend to be smaller in terms of both particle motion and change in energy. Figure 3c shows the relationship between particle motion Δ and energy change ΔE directly.

The number of particles participating in each rearrangement, N_p , can be measured by calculating the participation ratio of the displacements [27]. While N_p varies widely from ~ 1 to more than half of the system size, it does not appear to correlate especially well with the quantities shown in Fig 3. The exception is rearrangements with $N_p \approx 1$. These behave somewhat differently from other rearrangements as highlighted in Fig 3b; the moving particle in these events tends to correspond to a buckler [25]. See [11] for details.

Hysteron core — We quantify the core of a given rearrangement pair by determining how many particles are needed to switch between the two stable configurations as a function of strain between γ^- and γ^+ . At each strain value tested (see [11]), we rank the particles by difference in positions between the two configurations, referred to as $(-)$ and $(+)$. Starting in the $(-)$ configuration, we move

the particle with the largest difference to its position in the $(+)$ configuration and minimize. We then reset to the $(-)$ configuration and repeat, now moving the *two* particles with the largest differences in positions, then again with three, and so on. For each minimization, we test whether we have landed in the $(+)$ configuration. The smallest number of particles needed to push the system into the $(+)$ configuration gives us an estimate of the core size N_{core} .

In general, the transition is well behaved: for fewer than N_{core} particles moved, the system lands in the $(-)$ well, while for N_{core} or more particles, the system falls into the $(+)$ well. Occasionally, however, ($\sim 10\%$ of packings), the system lands in a third well for some intermediate number of particles. These packings are excluded from the calculation of average N_{core} values.

Figure 4 shows the number N_{core} of particles in the core for varied amounts of hysteresis (a) and for different system sizes (b). Each curve is averaged over several packings (see [11] for details) and shown as a function of $\gamma^* \equiv (\gamma - \gamma^-)/\gamma_h$. To average over hysteresis, rearrangement pairs are sorted based on the amount of hysteresis exhibited γ_h and averages are performed only over hysteron pairs with similar values of γ_h .

In all curves, the average number of particles needed to be manually moved in order to cause the rearrangement from $(-)$ to $(+)$ varies substantially as γ^* is varied. N_{core} approaches a substantial fraction of the particles far from the rearrangement and approaches one particle near the rearrangement. The equivalent measurement in the other direction, from $(+)$ to $(-)$, is on average identical when flipped about $\gamma^* = 0.5$.

Figure 4c shows the effect of scaling each system size curve by a different constant N_{fit} to collapse the data. This reveals that the shape of the curve changes only slightly with system size, N . For varied hysteresis, Fig. 4a, no rescaling is needed for collapse.

Discussion — Finding a single reversible plastic event is seemingly at odds with the idea of a jammed packing as a deeply complex glassy system. Yet our results indicate that such double wells not only exist but are in fact relatively easy to find.

Requiring that a rearrangement *immediately* be undone underestimates the probability that a rearrangement *can* be undone, particularly for larger system size — this may help explain the measured decrease in probability of finding a pair for large systems, shown in Fig. 2a. It also tends to bias the pairs found toward short hysteron pairs: the probability of a pair of rearrangements being “interrupted” by another rearrangement between them is larger for a pair of rearrangements with large γ_h . The chances of interruption grow as the number of possible instabilities increases, for example due to larger system size, biasing the whole distribution toward lower values of γ_h as indicated by Fig. 2c.

The strong overlap in statistics of rearrangements between paired and unpaired instabilities shown in Fig. 3b is consistent with the idea that rearrangements are gener-

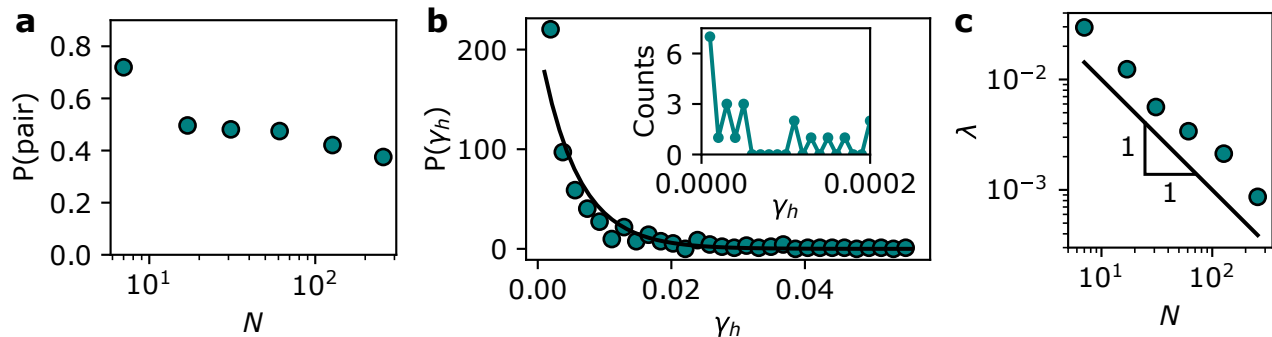


FIG. 2. Statistics of paired rearrangements ($\phi = 0.87$ and $\Delta\gamma = 10^{-3}$ except for the inset to (b)). (a) Probability $P(N)$ that a packing immediately falls into a two-rearrangement periodic orbit versus system size N . (b) Probability distribution function for a rearrangement pair to be separated in strain by hysteresis γ_h overlaid by an exponential fit (black line). Inset: Unbinned counts for $\Delta\gamma = 10^{-5}$ and $\phi = 0.99$. (c) Characteristic decay strain of hysteresis γ_h , obtained from fitting (b) to an exponential, versus N . Line is a guide to the eye with slope -1.

ically reversible, whether or not they are undone by the first rearrangement encountered upon reversing the direction of shear. Combined with the high probabilities shown in Fig 2a, this provides evidence that rearrangement pairs are a fundamental and prevalent aspect of amorphous materials.

Because of their origins in the magnetic materials community [12], hysterons are typically treated as spin-like objects. While this simple binary picture has been useful in attempts to understand general features of cyclically sheared amorphous solids, we show here that it does not hold up under closer scrutiny. In particular, attempts to isolate the particles responsible for switching the system between states as in Fig. 4 show that there exists no fixed subset of particles that constitutes the “hysteron” at all strains. Instead, the number of particles needed to cause the rearrangement varies dramatically as a function of strain.

A simple modification can partially rectify this picture: rather than considering spins, which generally have no internal structure, the local energy landscape can give insight into behavior at an instability. Information about the shape of the potential makes it possible, for instance, to predict the relationship between global quantities like the energy drop ΔE and the root-mean-squared displacement Δ associated with a rearrangement. Assuming a so-called fold instability of the type shown in Fig. 1a, the generic form of the energy at an instability ($\gamma = \gamma^+$, for example, and for particle configurations near the initial marginally stable equilibrium) is

$$E = -\alpha\Delta^3, \quad (1)$$

where α is a constant and Δ is the root-mean-square distance away from the initial unstable configuration (see, for example, [28]). Assuming that the instability is cut off randomly, for example due to newly formed contacts, this cubic behavior will dominate so that the behavior of an ensemble of packings will be $\Delta E \sim \Delta^3$, or $\Delta \sim \Delta E^{1/3}$.

While this appears consistent with the results seen in Fig. 3c, estimates of the potential energy as the system falls from one (barely unstable) well to the other show that a cubic fits only over a small fraction of the total distance travelled. This is shown in the SI [11]. This suggests that the fold instability is *not* at the heart of the systematic trends observed in Fig. 3. In addition, as shown in [11], a full quartic model, which takes into account the presence of a second minimum, predicts scalings that give a power law with exponents $1/4$ and $1/5$ depending on the potential, clearly inconsistent with Fig. 3. This, combined with the large range of participation ratios, indicates that instabilities are collective in nature. The trends between Δ , ΔE , and γ_h are clearly present yet may not be described by a simple power law. The relationships between these different parameters, as we report here, are essential to understanding the nature of shear instabilities in disordered materials. However, they remain unexplained.

While a third-order (cubic) potential may describe the initial behavior at an instability, more generally we can consider each hysteron to be a double well (quartic) energy potential modulated by the external strain γ so that one well disappears above γ^+ and the other disappears below γ^- . Such potentials, shown schematically in Fig. 1a, give rise to hysteresis generically, as the system is bistable for $\gamma^- < \gamma < \gamma^+$ but can be flipped between the two states by going to extreme strain values. If we consider the number of particles N_{core} needed to push the system from one well to the other to be a proxy for the energy-barrier height, it is no surprise that this quantity might be large for one strain (that is, when the current configuration is quite stable) and small for another (when the configuration is only marginally stable).

A double-well potential requires more information, namely the depth of each well and height of the barrier as a function of strain, compared with a hysteretic spin, which is defined by just two values γ^+ and γ^- . It would be interesting to restore additional double-well in-

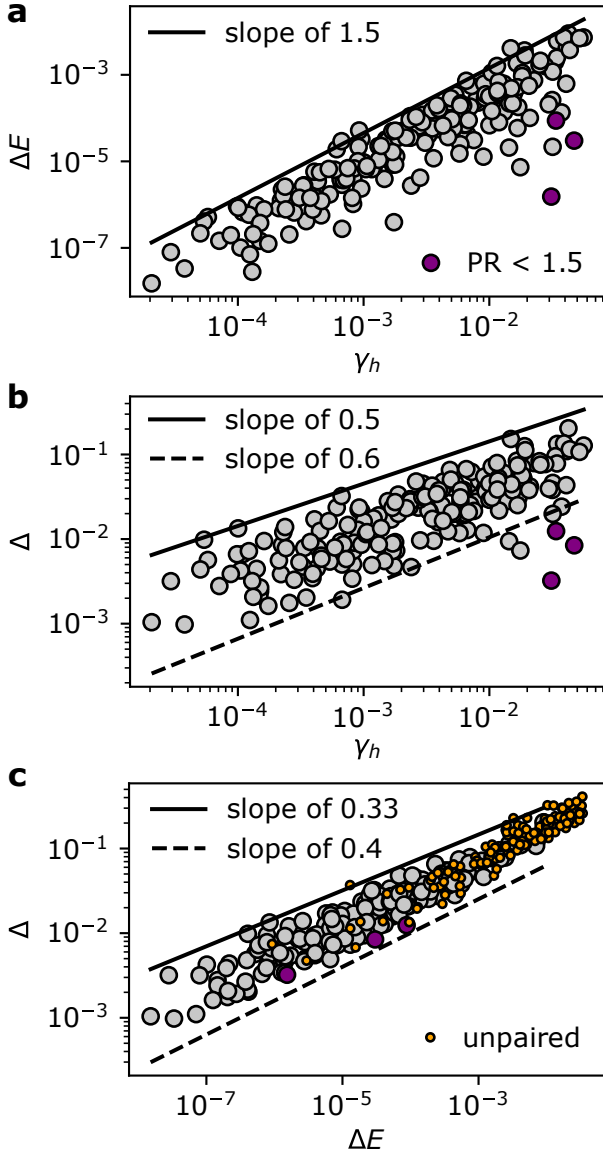


FIG. 3. Scaling between different features associated with rearrangements ($N = 31$ and $\phi = 0.95$). Lines are guides to the eye intended to bound the data. (a) Energy drop and (b) root-mean-square displacement Δ for hysteron rearrangements measured at γ^+ versus hysteresis γ_h . (c) Root-mean-square displacements Δ versus energy drop ΔE for the same rearrangements (large grey circles) and for rearrangements which were not undone by the first rearrangement encountered upon changing direction of shear (small orange circles). The overlap and similar slope between the paired and unpaired data indicate that the instability associated with one of the pairs in a hysteron is essentially indistinguishable from instabilities that are unpaired with any other instability nearby in strain.

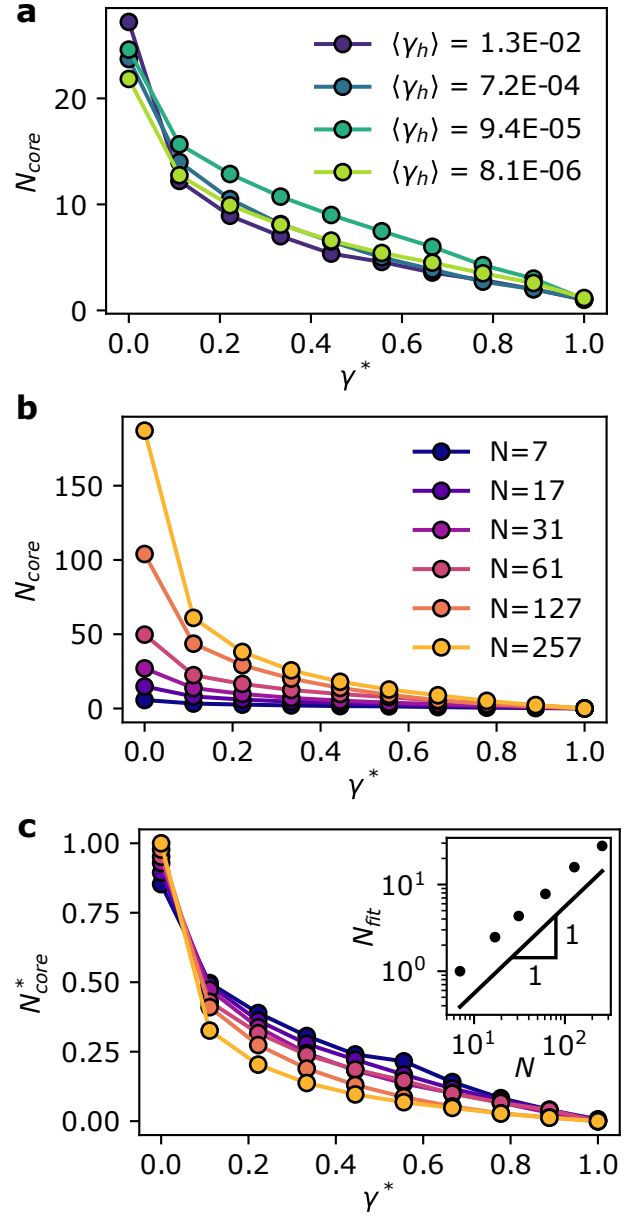


FIG. 4. Number of particles N_{core} needed to push the system from one configuration to another versus rescaled strain between the two rearrangements ($\phi = 0.95$) for (a) curves separated by amount of hysteresis γ_h with fixed system size $N = 31$ and (b) as a function of system size N . (c) As in b, but with each curve rescaled for collapse by a value N_{fit} (resulting y axis values in arbitrary units). Inset shows values used to rescale; line is a guide to the eye with slope 1.

formation to a simple hysteron model and explore the new features that emerge. The addition of temperature, for instance, is more natural in a double-well model where the barrier height is known.

However, even this double-well picture breaks down in light of the third energy minimum sometimes accessed when moving particles from one configuration to another.

It is an open question whether multi-state hysterons (that is, hysterons with more than two states) are distinguishable from interacting two-state hysterons [29] and, if so, what role such “hysterons” play in jammed systems.

The lack of clear separation between the core and dressing of rearrangement pairs, as well as instances of three-well scenarios as described above, suggests that binary spin hysterons are an inadequate model for paired rearrangements in sheared packings. In particular, these features suggest that pairs that are allowed to interact may do so in a very complicated way, with multiple internal states and subtle changes in one set of particles affecting others. How then do packings fall into periodic orbits quickly, even when many rearrangements are involved in a single cycle? We suggest that it is the statistics of pairs that restores an effective simplicity.

Interacting pairs tend to scramble one another, delaying the onset of periodicity [23]. Yet to interact, rearrangements need be not only within elastic range of each other spatially but also overlapping in strain. Figure 2b shows that most rearrangement pairs exhibit very little hysteresis (small γ_h), making overlap with other rearrangement pairs, and hence interactions, unlikely. With few interactions, the resulting dynamics remain relatively simple, with short transients.

Finally, our results also offer insight into global features of the energy landscape associated with jammed packings. Though known to be extraordinarily rugged, for a small system there may be the expectation that the amount of shear required to undergo a rearrangement — one measure of the distance to an instability — will be set by the particle size relative to the box length. Yet a two-dimensional system of 31 particles corresponds to a fractional particle size which is roughly $1/30^{1/2} \sim 0.18$,

at odds with the proliferation of γ_h values on the order of 10^{-5} . Moreover, the similarity of rescaled N_{core} behavior independent of hysteresis amount, shown in Fig. 4a (and hence rearrangement size in terms of both energy drop and mean displacement of particles) suggests a kind of self similarity between double wells across a range of scales. For a finite system, this cannot continue down to infinitesimal scales, as there is a finite though enormous number of total energy minima; further work is needed to determine what sets the minimum hysteresis scale.

We have shown that rearrangement pairs in jammed systems are inadequately described by binary, spin-like objects. Instead, we suggest that double-well energy potentials better capture the additional complexity of rearrangement pairs. However, pairs themselves are common and tend to exhibit very little hysteresis, features that may help explain why systems are able to fall into periodic orbits with relative ease but which complicates numerical and potentially even experimental studies in which smaller and smaller rearrangement pairs become more and more difficult to capture. Additional studies are needed to understand the abundance of low-hysteresis rearrangement pairs and their implications for real granular materials.

ACKNOWLEDGEMENTS

We thank Eddie Bautista, Eric Corwin, Varda Hagh, Martin van Hecke, and Lisa Manning for discussions. This work was supported by the US Department of Energy, Office of Science, Basic Energy Sciences, under Grant DE-SC0020972. C.W.L. was supported in part by NSF Graduate Research Fellowship Grant DGE-1746045.

-
- [1] N. C. Keim, J. D. Paulsen, Z. Zeravcic, S. Sastry, and S. R. Nagel, *Rev. Mod. Phys.* **91**, 035002 (2019).
 - [2] N. C. Keim and P. E. Arratia, *Soft Matter* **9**, 6222 (2013).
 - [3] I. Regev, T. Lookman, and C. Reichhardt, *Phys. Rev. E* **88**, 062401 (2013).
 - [4] D. Fiocco, G. Foffi, and S. Sastry, *Physical Review E* **88**, 020301 (2013).
 - [5] N. Perchikov and E. Bouchbinder, *Physical Review E* **89**, 062307 (2014).
 - [6] N. C. Keim and P. E. Arratia, *Physical review letters* **112**, 028302 (2014).
 - [7] D. Fiocco, G. Foffi, and S. Sastry, *Phys. Rev. Letts.* **112**, 025702 (2014).
 - [8] J. R. Royer and P. M. Chaikin, *Proceedings of the National Academy of Sciences* **112**, 49 (2015).
 - [9] M. O. Lavrentovich, A. J. Liu, and S. R. Nagel, *Phys. Rev. E* **96**, 020101 (2017).
 - [10] M. L. Falk and J. S. Langer, *Phys. Rev. E* **57**, 7192 (1998).
 - [11] See Supplemental Material at [URL will be inserted by publisher].
 - [12] F. Preisach, *Zeitschrift für Physik* **94**, 277 (1935).
 - [13] J. P. Sethna, K. Dahmen, S. Kartha, J. A. Krumhansl, B. W. Roberts, and J. D. Shore, *Phys. Rev. Letts.* **70**, 3347 (1993).
 - [14] M. Mungan, S. Sastry, K. Dahmen, and I. Regev, *Phys. Rev. Letts.* **123**, 178002 (2019).
 - [15] N. C. Keim, J. Hass, B. Kroger, and D. Wieker, *Phys. Rev. Research* **2**, 012004 (2020).
 - [16] M. M. Terzi and M. Mungan, *Phys. Rev. E* **102**, 012122 (2020).
 - [17] M. van Hecke, *Phys. Rev. E* **104**, 054608 (2021).
 - [18] A. Szulc, M. Mungan, and I. Regev, *J. Chem. Phys.* **156** (2022).
 - [19] D. Shohat, D. Hexner, and Y. Lahini, *Proceedings of the National Academy of Sciences* **119**, e2200028119 (2022).
 - [20] H. Bense and M. van Hecke, *Proceedings of the National Academy of Sciences* **118**, e2111436118 (2021).
 - [21] M. Mungan, *Proceedings of the National Academy of Sciences* **119**, e2208743119 (2022).
 - [22] N. C. Keim and J. D. Paulsen, *Science Advances* **7**, eabg7685 (2021).
 - [23] C. W. Lindeman and S. R. Nagel, *Science Advances* **7**, eabg7133 (2021).

- [24] P. K. Morse and E. I. Corwin, Physical review letters **112**, 115701 (2014).
- [25] P. Charbonneau, E. I. Corwin, G. Parisi, and F. Zamponi, Physical review letters **114**, 125504 (2015).
- [26] D. Xu, S. Zhang, A. J. Liu, S. R. Nagel, and N. Xu, Proceedings of the National Academy of Sciences **120**, e2304974120 (2023).
- [27] L. E. Silbert, A. J. Liu, and S. R. Nagel, Physical Review E **79**, 021308 (2009).
- [28] N. Xu, A. J. Liu, and S. R. Nagel, Physical review letters **119**, 215502 (2017).
- [29] C. W. Lindeman, V. F. Hagh, C. I. Ip, and S. R. Nagel, Phys. Rev. Letts. **130**, 197201 (2023).

Supplementary Material for “Minimal cyclic behavior in sheared amorphous solids”

(Dated: March 5, 2024)

APPLICATION OF SHEAR

The lattice vectors (LV), which define the periodicity of the lattice, are defined as follows:

$$LV = \frac{1}{\sqrt{1 - \gamma^2/4}} \begin{bmatrix} 1 & \gamma/2 \\ \gamma/2 & 1 \end{bmatrix} \quad (S1)$$

Note that this is volume preserving (that is, $\det(LV) = 1$ for all γ) and symmetric (*i.e.*, what is typically called simple shear).

DETECTING A REARRANGEMENT

We tested three metrics for determining whether a rearrangement has occurred. Two are introduced in the main text. Fig. S1 shows the equivalent distributions as those in Fig. 1 for a third metric: difference in energies between *sequential* frames (rather than the scheme outlined in the inset to Fig. 1b). This third metric, which we term ΔE_{seq} , also fails to clearly separate rearrangements from non-rearrangements

Fig. S1(b) shows the same values of ΔE , now as a function of the D_{min}^2 value, originally defined in [?], for the same set of frames. We choose as neighbors particles which are within a radius of $1.5\langle r \rangle$, where $\langle r \rangle$ is the mean particle diameter. Fig. S1(c) likewise shows ΔE versus the change in energy from one frame to the next ΔE^{seq} , respectively. In both cases, a continuous range of the x -axis variable means it would be impossible to identify with certainty when a rearrangement has occurred.

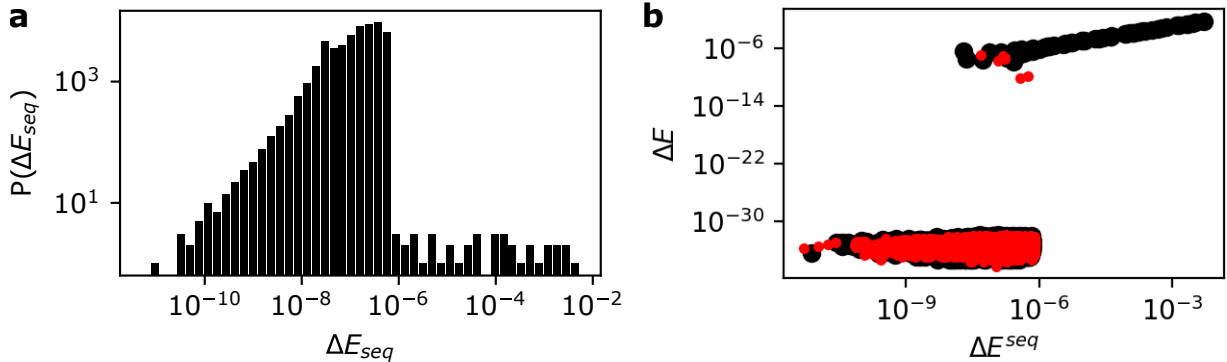


FIG. S1. (a) Probability distribution for the change in energy ΔE_{seq} between sequential values of applied strain. These are for the same set of events shown in Fig 1 of the main text, with $N = 31$, $\phi = 0.87$, and $\Delta\gamma = 10^{-5}$. Distribution includes only energy drops. (b) Direct comparison between ΔE (compared for like values of γ as in the main text) and ΔE_{seq} . Energy drops are shown in black while energy increases are shown in red. Note that energy increases corresponding to rearrangements are rare and an effect of finite step size.

Isolating γ^+ and γ^-

After a rearrangement pair (or unpaired rearrangement) was found using the above method, the endpoints γ^+ and γ^- were found with higher resolution using a bisection algorithm: if the original search algorithm found a rearrangement between 2×10^{-4} and 3×10^{-4} , the bisection algorithm checks between 2×10^{-4} and 2.5×10^{-4} to isolate the rearrangement strain with a resolution that is half the original step size. This was done iteratively until the value of the flipping strains were known with a resolution of 10^{-7} or less. These improved endpoints were then used for measurements of the energy drop ΔE , root mean square displacement of particles Δ , and hysteresis γ_h shown in Fig. 3, as well as for the calculation of the participation ratio.

Particle displacements

The root-mean-square particle displacement Δ , defined in the main text, was calculated after mapping the particles back to a square box configuration using the inverse of the lattice vectors. Particles which were rattlers (ie, have no stable contacts) before and/or after the rearrangement were excluded from the calculation and the drift, or average motion of all the particles, was subtracted off.

ANALYTICAL RESULTS

Using a simple spring model for a bistable (double-well) system, we can analytically work out a prediction for scaling behavior between particle displacement Δ , energy drop ΔE , and the hysteresis γ_h . This is possible for both harmonic and hertzian springs; neither reproduces the results seen in the main text. We suspect that this is because, while the instability itself may be accurately described by these models, the second minimum into which the system falls is an artifact of having springs that can exhibit both repulsive and attractive forces. Evidently in jammed systems, the second minimum is given by more complex many-body frustration that cuts off the locally cubic instability, as suggested in the main text.

Harmonic potential

To study an instability analytically, we treat the spheres as springs with fixed connectivity and consider the case of just two spheres sliding past each other. For harmonic springs, which store energy as the square of the compression $E \propto \delta x^2$, this corresponds to the simple bistable spring system introduced in [?], with exact energy

$$E(x, \gamma) = (\sqrt{(1 - \epsilon)^2 + x^2} - 1)^2, \quad (\text{S2})$$

where length and force have been non-dimensionalized by the spring's rest length and stiffness. For small compression ϵ and sliding motion x this becomes:

$$E(x, \gamma) = \frac{x^4}{4} - \epsilon x^2 + \gamma x, \quad (\text{S3})$$

where γ is the external field that pushes the two spheres past each other. This creates a double well potential which is perfectly symmetric at $\gamma = 0$ and becomes unstable at some critical external field value $\pm\gamma_c$.

We can relate the global parameters measured in the main text to features of this spring model: the root mean squared displacement Δ of a packing is the change in position Δx as the system falls from one minimum to the other, the energy drop ΔE of the packing is the difference in energy between the two wells, and the hysteresis γ_h is the external field difference between the left minimum going unstable and the right minimum going unstable. Based on the definition of γ_c above, the hysteresis is $2\gamma_c$.

Each of these can be worked out precisely in the spring model. The critical field γ_c occurs when the largest gradient in energy (i.e., maximum force) is offset by the external field. This will occur at a value $x_c = \sqrt{2\epsilon/3} \sim \epsilon^{1/2}$, determined by setting

$$-\frac{d^2E}{dx^2} = -3x_c^2 + 2\epsilon = 0. \quad (\text{S4})$$

The external field γ_c that must be applied to precisely balance this force is then

$$-\left.\frac{dE}{dx}\right|_{x=x_c} = -x_c^3 + 2\epsilon x_c, \quad (\text{S5})$$

giving $\gamma_c \sim \epsilon^{3/2}$. Finally, the energy drop associated with this instability is given by the difference in energy at the instability compared with at the minimum. The energy at the instability is just $E(x = x_c, \gamma = \gamma_c) \sim \epsilon^2$. The energy at the minimum can be found to scale the same way, so that the difference $\Delta E \sim \epsilon^2$. The position of this minimum likewise scales the same way as x_c so that $\Delta x \sim x_c \sim \epsilon^{1/2}$. Combining these three results, we see: $\Delta x \sim \gamma_c^{1/3}$, $\Delta E \sim \gamma_c^{4/3}$, and $\Delta x \sim \Delta E^{1/4}$. Recall that γ_c in this model is associated with γ_h in jammed systems, and Δx with Δ . This thus provides a prediction for all three power laws in Fig. 3. Though not far off, none are quite right.

Hertzian potential

Above, the argument about the scaling of Δ and ΔE with hysteresis made use of a simple spring model with an interaction potential going as overlap squared. Because the simulations reported are for particles with Hertzian interactions, however, we repeat the calculation for springs with power $5/2$.

In this case, the energy is

$$E(x, \gamma) = (\sqrt{(1 - \epsilon)^2 + x^2} - 1)^{5/2}, \quad (\text{S6})$$

and the expansion for small ϵ and x is

$$E(x, \gamma) \approx \frac{15\sqrt{\epsilon}}{32}x^4 - \frac{5\epsilon^{3/2}}{4}x^2 + \gamma x. \quad (\text{S7})$$

Using the same kind of analysis as above, we find the following predictions: $\Delta x \sim \gamma_c^{1/4}$, $\Delta E \sim \gamma_c^{5/4}$, and $\Delta x \sim \Delta E^{1/5}$. Compared with the harmonic results, these are further from the fits shown.

SIMULATION RESULTS FOR HARMONIC INTERACTIONS

We repeated simulations for $N = 31$ with harmonic interactions between particles at the same packing fraction used in the main text ($\phi = 0.87$). Note that this results in a much higher pressure compared with Hertzian packings at the same density. The resulting Δ and ΔE vs hysteresis plots are shown in Fig. S2. They are not statistically different from the equivalent plots for Hertzian potential, confirming that the interaction potential is not driving these scaling behaviors.

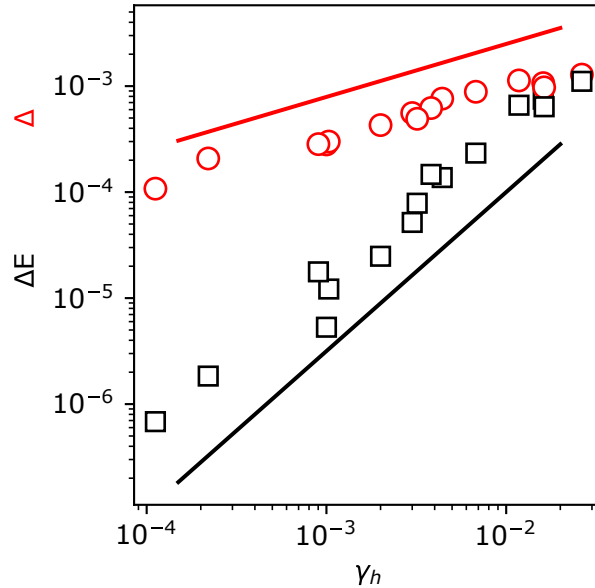


FIG. S2. (a) Root-mean-square particle displacements (red circles) and energy drop (black squares) of paired rearrangements as a function of the strain distance between the two rearrangements ($N = 31$ and $\phi = 0.87$). Each point is an average over the tops and bottoms of roughly 50 rearrangement pairs for $\Delta\gamma$ between 10^{-3} and 10^{-5} . Solid lines are the same as those in Fig. 3a of the main text (shown there with results for Hertzian springs): $1/2$ for Δ and $3/2$ for ΔE .

PARTICIPATION RATIO

If r_i is the distance each particle moves, the participation ratio of the motion is defined as

$$P = \frac{(\sum_i r_i^2)^2}{\sum_i r_i^4}, \quad (\text{S8})$$

a quantity which lies between $1/N$ and 1. The participation number N_p noted in the main text is then $N_p = P * N$.

Figure S3a shows the participation ratio, averaged over both rearrangements of several rearrangements pairs with similar hysteresis, as a function of averaged hysteresis. The participation ratio is roughly constant, around 0.4, over more than two orders of magnitude in hysteresis. This supports the claim in the main text that the participation ratio of rearrangements in a pair do not depend in a systematic way on the hysteresis of the pair.

The participation ratio does depend on the system size; when normalized by system size (so that it goes between 0 and 1 rather than 0 and N), it seems to fall logarithmically with N . This trend cannot continue forever; in the limit of large N , the participation ratio must plateau to zero.

Bucklers

Packings with participation number close to 1 (that is, only, one particle contributed to the rearrangement) tended to be bucklers; Figure 3 in the main text shows that the statistics of these packings are somewhat different from those with higher participation number.. Fig. S4 shows the rearrangement structure of one of these packings.

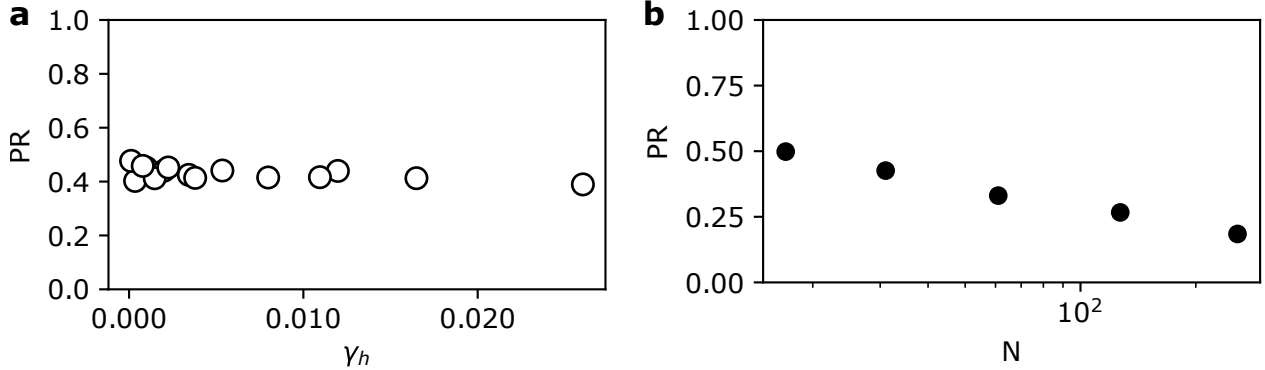


FIG. S3. (a) The participation ratio of paired rearrangements as a function of the strain distance between the two rearrangements. Each point is an average over the top and bottom of roughly 50 rearrangement pairs found with step size specified in the legend. ($N = 31$, $\phi = 0.87$). (b) The average participation ratio for all pairs found with $\Delta\gamma = 10^{-3}$ as a function of system size ($\phi = 0.87$).

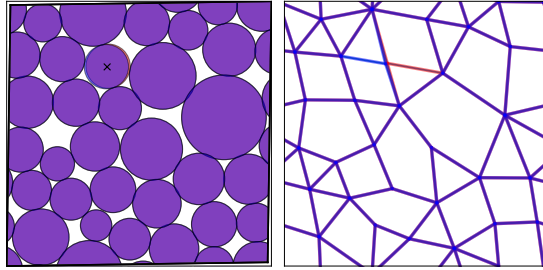


FIG. S4. Example of a rearrangement with low participation number, $N_p < 1.5$, with motion dominated by a buckler. Left: particle packing shown directly; red and blue show the configurations of the particles before and after the rearrangement, respectively, with most of the packing unchanged by the rearrangement and hence purple. Slivers of red and blue are just visible on either side of the buckler, which is marked with an x. Right: the associated contact network, colored as in (a), showing a single change in contact associated with the buckler buckling from left to right.

N_{core} MEASUREMENT

The full protocol for determining N_{core} as a function of strain is as follows. Starting from a rearrangement pair found as detailed in the main text, the values of the flipping strains γ^+ and γ^- was determined at a higher resolution $\Delta\gamma/100$ using a bisection algorithm. (For example, a pair originally found with resolution $\Delta\gamma = 10^{-3}$ would have flipping strain values with resolution of 10^{-5} .) This reduces packing-to-packing fluctuations in distance between endpoint measurements ($\gamma^* = 0$ or 1) and the instability.

Using the precise values of strain just “inside” either end of the hysteron, the strain distance was divided linearly into 10 points, including the “inside” endpoints. A measurement of N_{core} is then made at each of these points as described in the main text. Results shown are averaged over between 10 and 20 such measurements with the same value of N and initial $\Delta\gamma$.

Occasionally, approaching the endpoints via bisection resulted in a different value of the flipping strain compared with approaching it with larger steps (this is possible because of the small difference between particle positions before and after minimizing, even without a rearrangement; depending on the step size taken, the rearrangement may be triggered at a slightly different strain value than

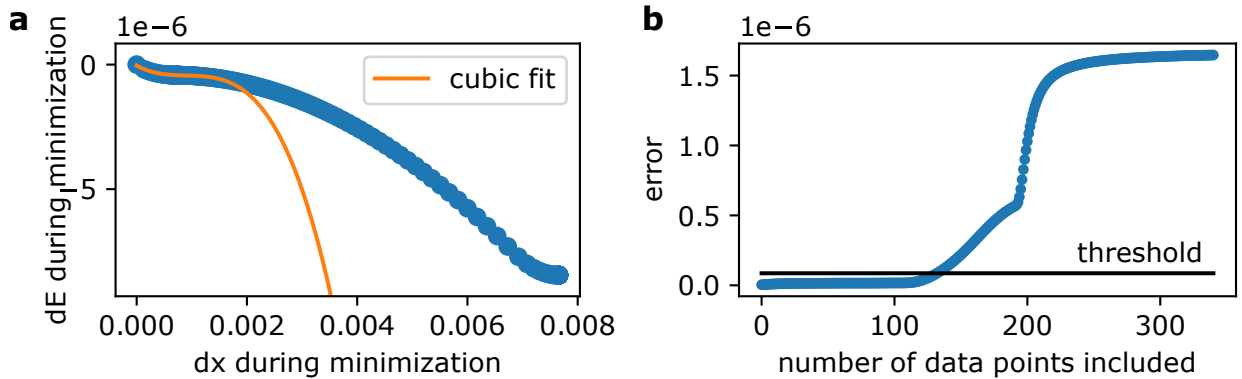


FIG. S5. (a) The position and energy during minimization over the course of an instability in a 31-particle packing with $\phi = 0.95$ and harmonic contacts. (b) The error of the cubic as a function of number of points included to fit in addition to the first 10 points. A threshold of 5% above the initial error is shown in black; this value was used to determine how many points to include in the fit shown in (a).

the “true” rearrangement strain expected for infinitesimal step size). These packings were excluded from N_{core} analysis but are expected to behave as those analyzed.

ESTIMATING THE POTENTIAL BETWEEN WELLS

To assess whether a fold instability (cubic function) could explain the scaling behavior seen in Fig. 3, we tracked the energy and particle positions during the minimization process as the system fell from one (marginally unstable) “minimum” to the other well. The process was halted at points evenly spaced in terms of number of steps and the positions and total energy recorded. The energy was then plotted as a function of distance from the initial configuration. A typical resulting “landscape” is shown in Fig. S5a.

Starting from the 10 data points closest to the initial configuration (leftmost point in the figure), we tested cubic fits each additional point, computing the error on the fits. As seen in Fig. S5b, the error is quite low for some fraction of the points, then begins to rise dramatically. By setting a threshold, in this case 5% increase in error, we can estimate how much of the x-range in Fig. S5a this cubic fit represents. Typically, this value was only a small fraction of the total distance from initial configuration to minimized configuration (less than 20% in the example shown; sometime only a few percent).